Raman spectroscopy and spreading resistance analysis of phosphorus implanted and annealed silicon

Andreas Othonos
Ontario Laser and Lightwave Research Center, University of Toronto, Toronto, Ontario M5S 1A7, Canada

Constantinos Christofides
Department of Natural Sciences, Faculty of Pure and Applied Sciences, University of Cyprus, P.O. Box 537, Nicosia, Cyprus

Joumana Boussey-Said
Laboratoire de Physique des Composants à Semiconducteur, URA CNRS 840, 23 rue des Martyrs, B.P. 257, 38031 Grenoble Cedex 1, France.

Michel Bisson
MITEL, Semiconductor Division, 18 Boulevard de l' Aeroport, Bromont, Québec JOE ILO, Canada

(Received 22 November 1993; accepted for publication 24 February 1994)

Raman and electrical characterization measurements are performed in order to study the effects of thermal annealing on phosphorus implanted silicon wafers. The silicon layers were implanted for various implantation energies and doses, below, and over the critical dose of amorphization. The post-implanted period was followed by thermal isochronal annealing at various temperatures. Special attention has been given to the amorphous/crystal transition occurring at various annealing temperatures. A bi layer model [R. Loudon, J. Phys. (Paris) **26**, 677 (1965)] has been used for a quantitative determination of the annealing temperature at which a complete annihilation of implantation defects takes place. For this analysis, Raman spectra, resistivity depth profiles, as well as 1D-SUPREM III simulation were used.

I. INTRODUCTION

Since the pioneering work of Gibbons[1,2] on ion implantation physics and technology several laboratories around the world have been working to solve, better understand, and explain some fundamental problems arising from the short and long range disorder created during ion implantation in semiconducting wafers. During the last three decades several experimental techniques for the characterization of such implanted materials have been developed. Some of these techniques have been very successful and today they are broadly used in many laboratories and high technology industries for destructive and nondestructive characterization of implanted and annealed wafers.

In a recent review paper, Christofides[3] summarized several results obtained by various techniques (electronic, physicochemical, optical, and thermal waves) in the field of ion implantation. That review paper emphasized the influence of annealing on the implanted layers. In fact the author noted that one problem which is still unsolved in this field is due to the confusion that exists between the activation of the implanted impurities and the evolution of structural properties of such inhomogeneous materials during an annealing process.

Raman spectroscopy could be very useful in solving the problem mentioned in the above paragraph. However, although very useful, Raman spectroscopy is not widely used in studying the annealing kinetics of defects in implanted semiconducting materials. Raman scattering was used in studies performed by Engstrom and Bates[4] as well as Forman *et al.*[5] who examined the damage created by ion implantation in boron-implanted and laser-annealed silicon wafers. In addition Kirillov *et al.*[6] used Raman scattering to study arsenic implanted and rapidly annealed (with a tungsten halogen lamp) wafers. Moreover in 1982, Nakamura and Katoda[7] used the same technique to study Si- and Sn-implanted GaAs wafers.

Some variations of this optical technique, for example resonance Raman spectroscopy on annealed He-, Na-, and Cd-implanted cuprous oxide have been performed by Hesse and Compaan.[8] Raman microprobe spectroscopic analysis has also been used by Nissim *et al.*,[9] among others, in order to study the defects in implanted silicon wafers annealed with picosecond laser pulses.

We believe that Raman spectroscopy has a lot more to offer in the characterization and full understanding of the damage caused by ion implantation as well as the annihilation process of this damage during annealing. Raman spectroscopy can be even more powerful when combined with electrical measurements. A good choice of an electrical characterization technique combined with Raman spectroscopy data could give a large amount of complementary information.

In fact, the classic electrical investigation, which is based only on sheet resistance analysis, cannot provide an accurate description of the defect annihilation mechanism since the defect profile is depth dependent. On the other hand, the spreading resistance technique provides an ideal tool for resistivity depth profile measurements.[10–13] Therefore, Raman spectroscopy, which can provide sub-surface information, is a very useful complementary technique for these studies.

In this work we characterize a large matrix of implanted silicon wafers using Raman spectroscopy and spreading resistance measurements. Section II refers to Raman spectros-

0021-8979/94/75(12)/8032/7/$6.00
© 1994 American Institute of Physics

Downloaded 08 Dec 2007 to 194.42.23.6. Redistribution subject to AIP license or copyright; see http://jap.aip.org/jap/copyright.jsp

copy and its nondestructive nature. Details of sample preparation are described in Sec. III. Section IV summarizes the experimental results while Sec. V gives a general critical discussion. Finally, a bi-layer model is used in the last section for the determination of the annihilation temperature for defects introduced by each implantation dose.

II. RAMAN SPECTROSCOPY AS A NON-DESTRUCTIVE TECHNIQUE

Raman spectroscopy can offer important information such as: (a) free-carrier concentration; (b) number of impurities in substitutional sites of the implanted lattice, and (c) crystalline/amorphous monitoring. Several years ago the appropriate theory concerning the Raman scattering in semiconducting silicon was analyzed by Fano.[14] Cerdeira has adapted the Fano theory to the case of boron-doped Si.[15] Baserman and Bernstein[16] have applied the theory in order to study boron-implanted silicon wafers after thermal annealing. Engstrom and Bates[4] modified the Fano model in order to determine the concentration of implanted boron in silicon. These authors pointed out the potential and limitations of Raman spectroscopy toward the characterization of ion implanted materials. They have extended the Fano theory in order to determine the concentration of impurities in ion implanted silicon wafers and obtained an excellent fitting of their experimental data in the case of implanted and unannealed layers. However, they had no success in their annealed samples. In fact, the well known problem related to the kinetics of annealing of short and long range disorder, as well as the variation of the degree of inhomogeneity (during annealing) of such materials makes the quantitative modelization a very difficult task even today.

Raman spectra obtained from ion implanted wafers consist of three components which correspond to: (i) the scattering from the crystalline substrate, (ii) the amorphous phase, and (iii) the mixed amorphous crystalline phase at the initial ***a*/*c*** interface. For our experimental measurements with the excitation laser light at 530.9 nm the **penetration depth**, δ, is estimated to be approximately 1.3 μm. This length basically determines the depth at which the Raman signal is probing. Therefore, the signal is only sensitive to changes in the sub-surface of the samples up to 1.3 μm. From this, it is easy to see that one may change the Raman probing depth by simply changing the wavelength of the excitation. Therefore, Raman spectroscopy could be considered as a nondestructive evaluation (NDE) technique. This will be examined in future work. For the time being, our measurements were obtained with a single wavelength (530.9 nm).

III. IMPLANTED SILICON SAMPLES

2-in.-diam silicon wafers lightly doped with boron (20–25 Ω cm) were implanted through a thin oxide layer at room temperature with phosphorus at various doses and energies (implantation dose: $\Phi=1\times10^{13}$ to 1×10^{16} P^+/cm^2; implantation energy: $E=20-180$ keV). The implantation process was made by MITEL Semiconductor Division at Bromot, Québec, Canada in 1992. After implantation the wafers were cut along the crystallographic axes into several

TABLE I. Junctions' depths of samples implanted with 150 keV at various doses [Φ (P^+/cm)], unannealed and annealed at various temperatures T_a (°C). The values of the first lines for each annealing temperature have been obtained from 1D-SUPREM III simulation, while the second line (in bold) were obtained from speading resistance measurements.

$\Phi(P^+/cm)$ T_a(°C)	1×10^{13}	1×10^{14}	5×10^{14}	1×10^{15}	5×10^{15}	1×10^{16}
NA	0.45	0.48	0.50	0.51	0.52	0.53
800	0.45	0.50	0.52	0.53	0.63	0.63
	0.48	**0.64**	**0.65**	**0.63**	**0.75**	**0.70**
850	0.46	0.49	0.53	0.52	0.75	0.80
	0.50	**0.65**	**0.65**	**0.67**	**0.80**	**0.80**
900	0.48	0.50	0.54	0.55	0.90	1.03
	0.60	**0.80**	**0.70**	**0.70**	**0.90**	**1.00**
950	0.53	0.57	0.60	0.60	0.97	1.45
	0.60	**0.85**	**0.80**	**0.75**	**1.10**	**1.50**
1000	0.63	0.72	0.75	0.78	0.97	1.90
	0.68	**0.90**	**0.90**	**0.80**	**1.30**	**1.50**
1100	1.32	1.55	1.70	1.74	2.03	2.40
	0.80	**1.15**	**1.51**	**1.52**	**1.81**	**2.59**

square samples of dimensions 1×1 cm^2. These samples were then thermally annealed isochronically at various temperatures (300, 350, 400, 500, 550, 600, 700, 800, 850, 900, 950, 1000, and 1100 °C) for 1 h in an inert nitrogen atmosphere. The withdrawal of the wafers from the furnace to the room-temperature environment was controlled automatically. After annealing, the oxide overlayer was etched away on samples which were used for Raman spectroscopic characterization while this oxide layer was kept on samples characterized by the spreading resistance method[10–12] in order to accurately determine the beginning of the overlayer resistivity profile.

IV. EXPERIMENTAL RESULTS

In this work as we mentioned earlier the Raman penetration depth is approximately 1.3 μm. We believe this is sufficient for probing our samples since it is comparable to the maximum depth of the amorphous layers created by ion implantation (see Table I). Table I presents the thickness of the *p-n* junction (in μm) for each dose and each annealing temperature. The values in the first line for each annealing temperature have been obtained from 1D-SUPREM III simulation while the second line (in bold) has been obtained from spreading resistance measurements. It is clear from the values in Table I that only samples implanted with doses over 5×10^{14} P^+/cm^2 and annealed at 1100 °C, as well as the ones which were implanted and annealed at 1000 °C, have thickness greater than δ. Therefore, Raman scattering with 530.9 nm light probes almost the total implanted volume of all the samples.

The various samples described in Sec. III were characterized by Raman spectroscopy at room temperature using

Downloaded 08 Dec 2007 to 194.42.23.6. Redistribution subject to AIP license or copyright; see http://jap.aip.org/jap/copyright.jsp

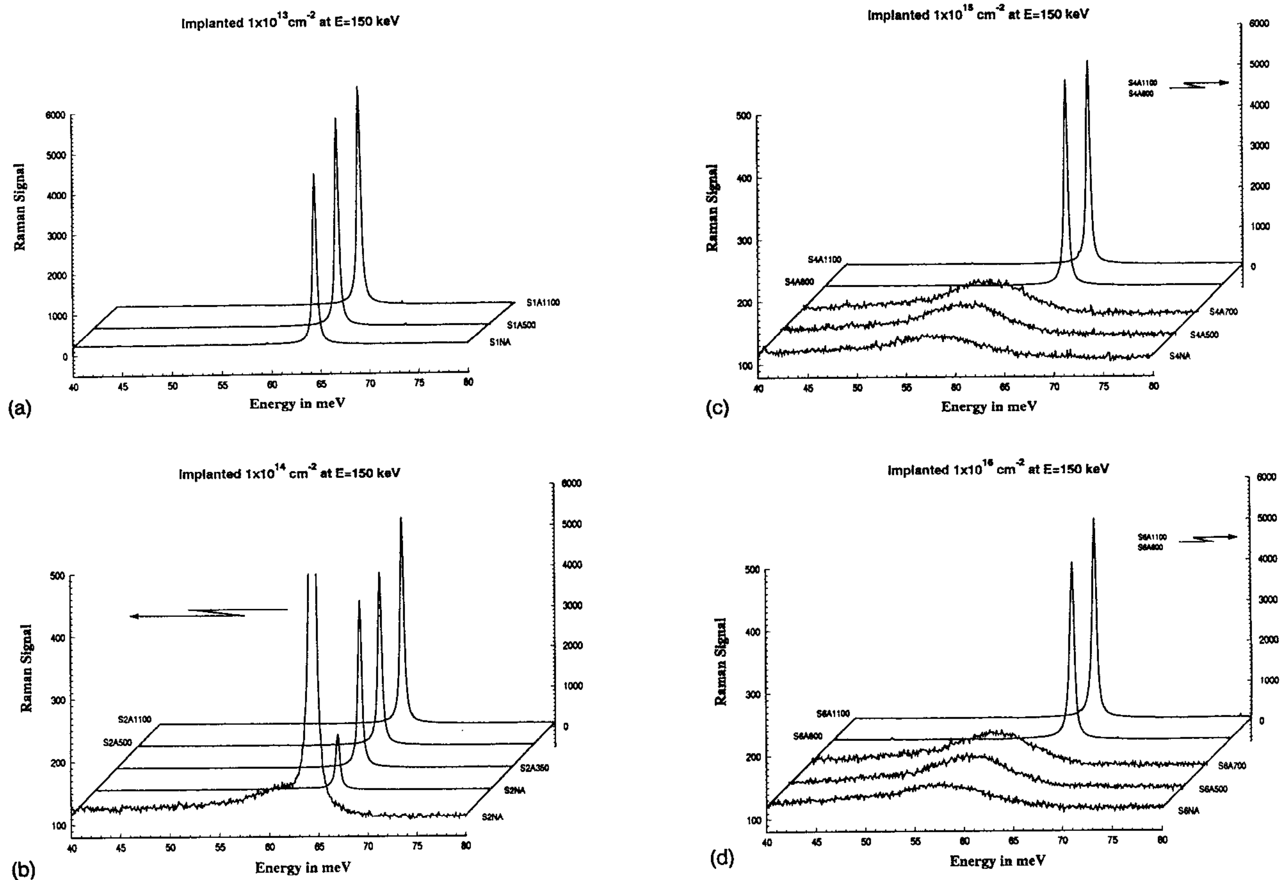

FIG. 1. Raman spectra from phosphorus implanted unannealed and annealed silicon samples (1: 1×10^{13}; 2: 1×10^{14}; 3: 5×10^{14}; 4: 1×10^{15}; 5: 5×10^{15}; 6: 1×10^{16} P^+/cm^2). The spectra were obtained at room temperature. The implantation energy was 150 keV and the implanted dose $|\Phi$ (P^+/cm^2): (a) $1|\times110^{13}$, (b) $1|\times10^{14}$, (c) $1|\times10^{15}$, and (d) $1|\times10^{16}$. The meaning of the labeling of the spectra (in Figs. 1 and 2): S stands for sample; the number stands for the implantation dose (1: $1|\times10^{13}$, 2: $1|\times10^{14}$, 3: $5|\times10^{14}$, 4: $1|\times10^{15}$, 1: $5|\times10^{15}$, 6: $1|\times10^{16}$ P^+/cm^2); A stands for annealed, NA stands for nonannealed, and the number after A stands for the annealing temperature.

the Kr laser line at 530.9 nm. Figures 1(a)–1(d) show a comparison of the Raman spectra of unannealed and annealed phosphorus silicon samples that were implanted at 150 keV with various doses [$\Phi(P^+/cm^2)$: 1×10^{13}, 1×10^{14}, 1×10^{15}, and 1×10^{16}]. The silicon optic phonon mode is visible through the large peak at 64.5 meV. Balkanski *et al.*[17] also reported similar values for the Raman active mode of crystalline silicon: 64.6 meV. Figures 2(a)–2(c) present several Raman spectra obtained from silicon samples implanted with a constant dose (5×10^{14} P^+/cm^2) at various implantation energies ranging between 20 and 180 keV.

In order to study the evolution of the electrical properties of such implanted samples with different annealing conditions, spreading resistance measurements have been performed and resistivity depth profiles have been obtained. The implantation induced damage on the local resistivity behavior for samples implanted at various doses with 150 keV phosphorus ions is shown in Fig. 3.

V. DISCUSSION AND ANALYSIS

A. Constant implantation dose

It is well known that Raman scattering from crystalline silicon results in a sharp feature due to the zone center optical phonon. In crystalline silicon the characteristic phonon peak occurs at approximately 64.5 meV (520 cm^{-1}) (Ref. 17) and this is exactly what we observe in our data for *c*-Si in the whole series of our Raman spectroscopic measurements. In addition to this, in Figs. 1(c) and (d) one can see (unannealed and low annealed samples) an acute broadening at 60 meV (483 cm^{-1}) which is due to the amorphization of the silicon surface after heavy implantation. The phenomenon occurs only for implantation doses above the critical amorphization dose, Φ_c (1×10^{15} P^+/cm^2).[18] The spectra presented in Figs. 1(a) and 1(b) corresponding to the lightly implanted samples do not exhibit such behavior. In fact, the broad feature that it is typical of amorphous materials disappears after annealing at 800 °C, where annihilation of many kinds of defects (interstitial, vacancies, point defects, complexes, dislocation lines and loops, and full amorphized layers) and recrystallization take place.[19,20] It should be noted that in amorphous materials there is a breakdown of the Raman scattering selection rules because of the absence of well defined crystal momentum (after implantation). The obtained Raman spectra no longer relate to the allowed optical phonons at the center of the Brillouin zone but rather to a convoluted function of the density of phonon states of the amorphous layer. This is

Downloaded 08 Dec 2007 to 194.42.23.6. Redistribution subject to AIP license or copyright; see http://jap.aip.org/jap/copyright.jsp

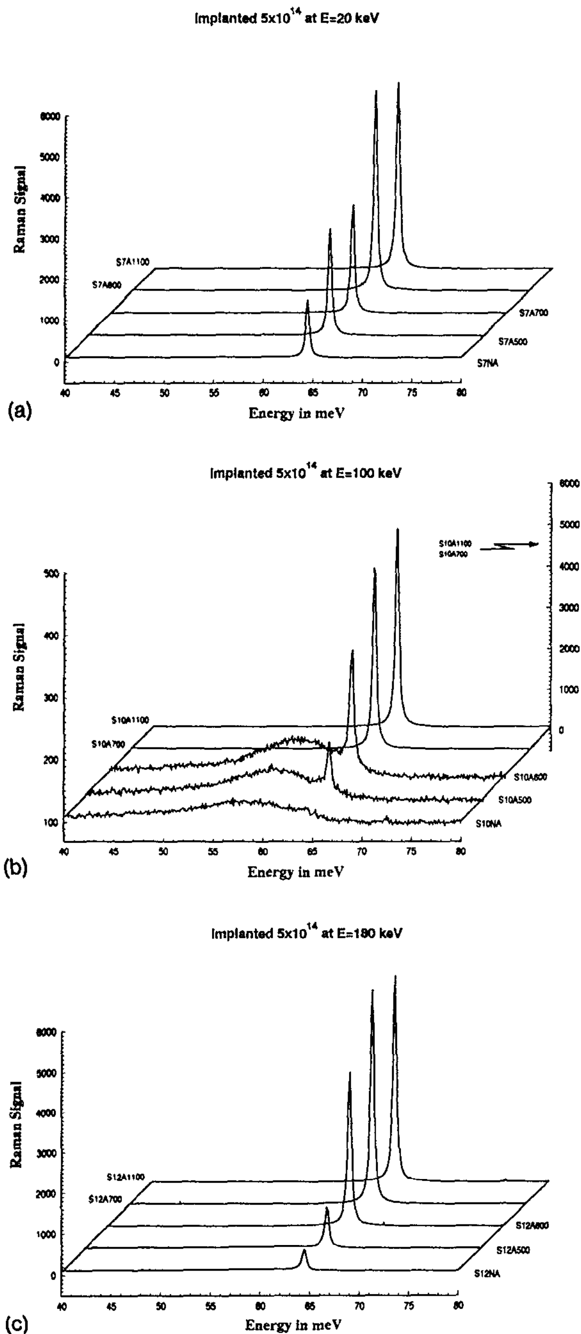

FIG. 2. Raman spectra from phosphorus implanted unannealed and annealed silicon samples. The spectra were obtained at room temperature. The implanted dose was 5×10^{14} P^+/cm^2 and the implanted energy E (keV): (a) 20, (b) 100, (c) 180.

another reason why Raman scattering is an excellent technique for NDE monitoring of crystalline/amorphous transitions.

To obtain a better understanding of our experimental results we have summarized the raw experimental data of Fig. 1 in Fig. 4. The results presented in this figure were obtained from samples implanted at 150 keV. Thus, the phonon peak intensities (PPI) are presented as a function of the implanted dose for various annealing temperatures. It is important to point out that in the case of samples annealed at high temperatures (800–1100 °C), the PPI does not vary significantly with annealing temperature for all implanted doses. Contrary to heavily implanted samples the PPI is almost constant with an annealing temperature for lightly implanted samples. On the other hand, the presence of an amorphized layer in the unannealed and low temperature annealed samples results in a considerable decrease of the PPI versus amorphization dose, Φ. In fact, since the implantation energy is constant, the damage will occur approximately over the same volume in all the samples. Therefore the phonon peak intensity will decrease when the dose increases until it reaches zero where we can only see a broad-band Raman signal due to amorphization.

Figure 5 shows another aspect of our summarized Raman results. In this figure one can see the variation of the phonon peak intensity versus annealing temperature. We would like to emphasize the following key points:

(i) A strong modification of the material appears to occur at about 700 °C for the heavily ion implanted samples.

(ii) All the samples, independent of their implantation dose, reach the recrystallization stage for annealing temperatures higher than 800 °C.

(iii) The recrystallization process on all the samples implanted with doses lower than the critical one, occurs in a smooth way. In fact, the annealing process in these samples is governed by different kinetics which have more to do with the migration of interstitial impurities and vacancies rather than the amorphous/crystalline transition.[20] The electrical behavior of samples presented in Fig. 3 confirms previous studies presented by other authors about the nonamorphization of silicon at this stage.[20,22]

(iv) Taking into account the spreading resistance results one notes that Figs. 3(a) and 3(b) present resistivity depth profiles obtained from samples implanted at 1×10^{13} and 1×10^{14} P^+/cm^2, respectively. Note that for those unannealed samples as well as the annealed ones at temperatures under <800 °C there is a high density of implantation induced point defects. A significant decrease of the resistivity is observed only after thermal annealing at temperatures over 800 °C. This heat treatment is expected to anneal the above mentioned defects and to allow dopant species to move toward substitutional sites in the implanted silicon lattice.

(v) When the implantation dose is higher than the critical amorphization dose ($\Phi_c=1\times10^{15}$ P^+/cm^2)[3] an amorphous overlayer is formed under the surface. This is evident from the measurements for the same samples reported by Christofides *et al.*[23] which gave an estimation of the width of the amorphous layer induced by the implantation.

(vi) Figures 3(c) and 3(d) show resistivity profiles obtained from samples implanted with 5×10^{15} and 1×10^{16} P^+/cm^2, respectively. The high resistivity surface layer for the unannealed samples is obvious in these figures. Contrary to the cases presented in Figs. 3(a) and 3(b) a low temperature annealing (see 350 °C) is sufficient to make the surface resistivity drop drastically by more than 3 orders of magnitude.

(vii) Diffusion effects are visible for all doses after annealing at 1100 °C.

(viii) The phonon peak intensity seems to be very sensitive to the effect of implantation even for samples implanted

Downloaded 08 Dec 2007 to 194.42.23.6. Redistribution subject to AIP license or copyright; see http://jap.aip.org/jap/copyright.jsp

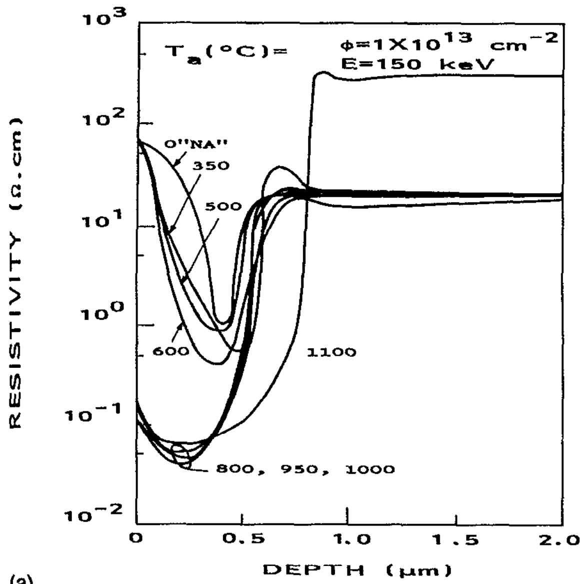

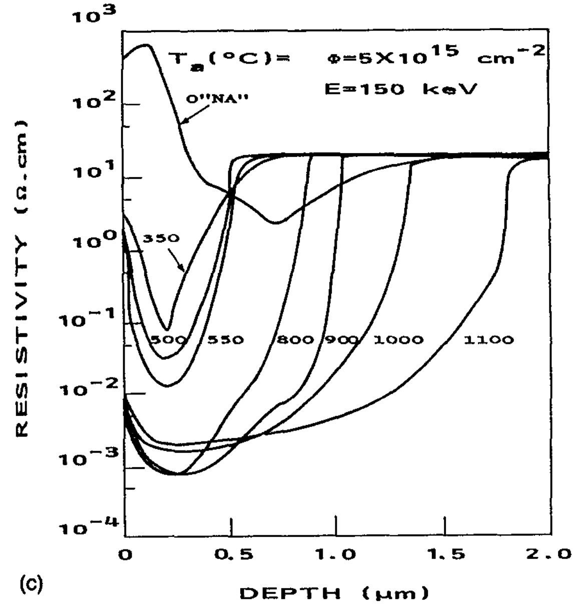

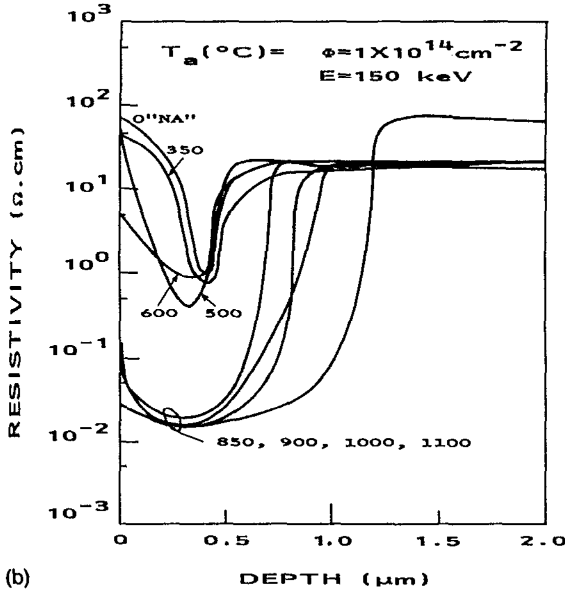

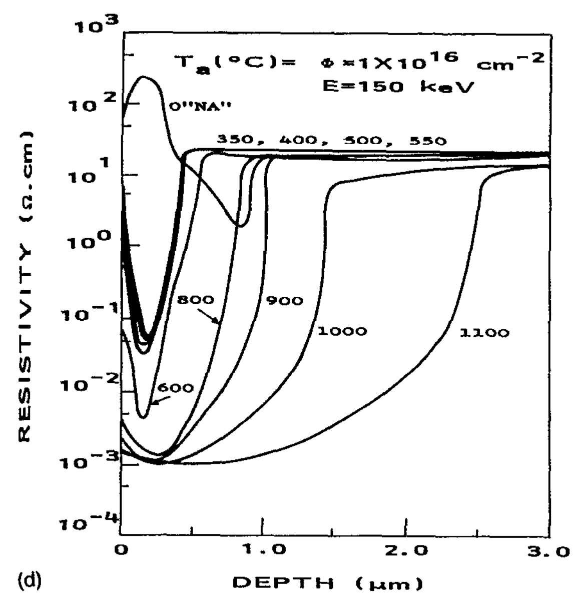

FIG. 3. Resistivity profiles of the phosphorus implanted (150 keV) silicon layers obtained by spreading resistance measurements for various implanted doses $|\Phi(P^+/cm^2)$: (a) $1|\times 10^{13}$, (b) $1|\times 10^{14}$, (c) $5|\times 10^{15}$, and (d) $1|\times 10^{16}$.

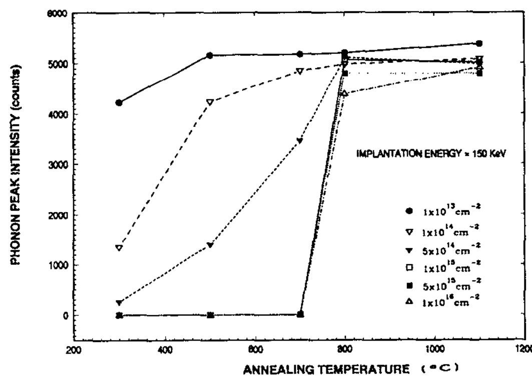

FIG. 4. Raman peak intensity of spectra as a function of annealing temperatures for various implanted doses (data obtained from Fig. 1). Implantation energy: 150 keV.

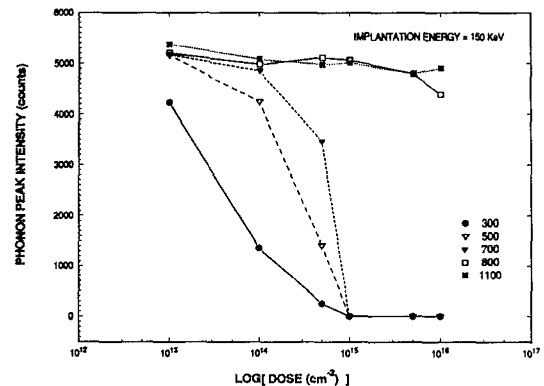

FIG. 5. Raman peak intensity of spectra as a function of the implanted dose for various annealing temperatures (data obtained from Fig. 1). Implantation energy: 150 keV.

Downloaded 08 Dec 2007 to 194.42.23.6. Redistribution subject to AIP license or copyright; see http://jap.aip.org/jap/copyright.jsp

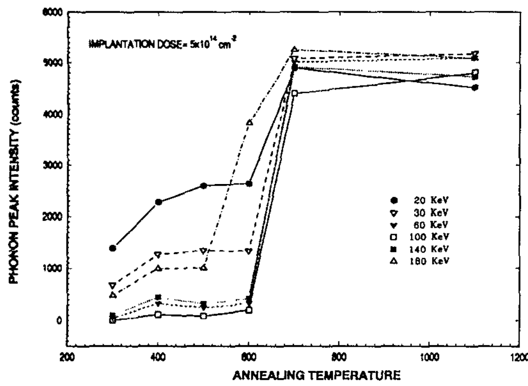

FIG. 6. Raman peak intensity of spectra as a function of implantation energy for samples implanted at 5×10^{14} P^+/cm^2 and annealed at 1000 °C.

at very low dose such as 1×10^{13} P^+/cm^2. For such samples the defect annihilation process continues to take place even for annealing temperatures higher than 800 °C. This may be due to the fact that the annihilation of defects in the layer is much more efficient in the case where an amorphous layer has been formed.[20,21]

B. Constant implantation dose

Figure 6 shows the plot of the phonon peak intensity as a function of the annealing temperature for the various implantation energies. These data were obtained from the experimental results presented in Fig. 2. In Fig. 6 one can see that the sharp Raman phonon peak intensity decreases as the energy of ion implantation increases from 20 to 100 keV. However, for high implantation energies (140–180 keV) the variation of the Raman scattering is not monotonic as it would have been expected. This can be explained by the fact that the implanted layers contain two types of damages: (a) amorphization of the layer, including the dislocation lines and loops of the lattice and (b) interstitial implanted impurities. A closer look at Fig. 6 suggests that at low implantation energies (20–100 keV) the Raman signal is due to the global implanted volume since the penetration depth is larger than the depth of the implanted layer (see Table I). On the other hand, for higher implanted energies (140–180 keV) where the thickness of the implantation layer becomes larger than the Raman penetration depth, some of the implanted impurities are no longer within δ; therefore the contribution of these impurities will become less important. In fact, once the implanted ions are deeper than the penetration depth their contribution to the Raman signal will only be from the amorphization of the silicon crystal.

VI. QUANTITATIVE ESTIMATION OF ANNIHILATION TEMPERATURE

The evolution of the n-p junction depth during the annealing process can be determined by several techniques. In this work we estimate the depth of the amorphized (and/or highly damaged) implanted and annealed samples with 1D-SUPREM III simulations. These simulations include data from spreading resistance measurements and by reflectance

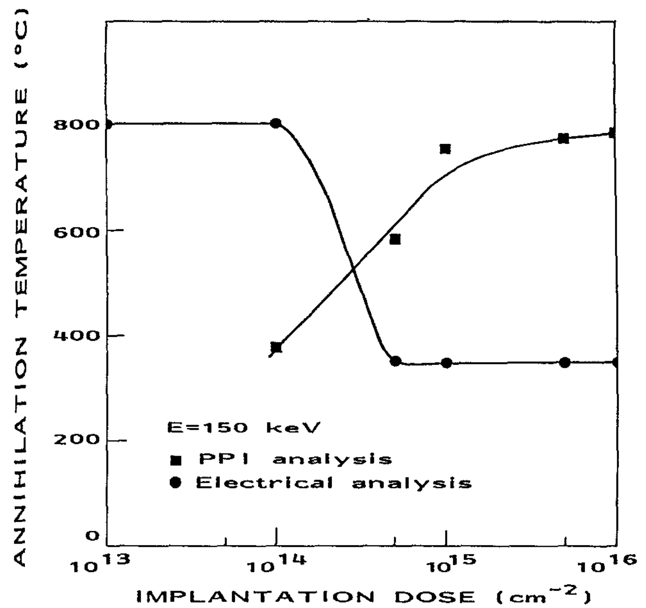

FIG. 7. Variation of the annihilation temperature as a function of the implanted dose.

measurements obtained by Christofides *et al.*[23] From the work of Loudon,[24] the ratio of Raman signal intensities for optically opaque materials is given by the relation:

$$\frac{I_i}{I_s}=\frac{R_i}{R_s}\frac{a_i}{a_s}\exp(2\ a_iL_i-1),$$

where I_i, R_i, α_i, and I_s, R_s, α_s are the intensities at the Raman shift frequency, the scattering coefficients, and the optical absorption coefficients of the implanted layer and the substrate, respectively. Kirillov *et al.*[6] have used the above equation in order to calculate the thickness of the implanted layer, L_i. These authors assumed that the absorption coefficient for incident and scattered light have the same values and that they are much larger than the scattering coefficient. This is considered to be a good approximation. Thus, R_i/R_s was estimated to be approximately 0.25; this estimate was made by taking into account the results of Kirillov *et al.*[6]

The use of the above equation combined with the SUPREM III simulation and spreading resistance results allowed us to determine the variation of the defect-annihilation temperature versus implantation dose (Fig. 7). The following steps and assumptions were made in order to calculate these temperatures: Since the above equation is proposed only for a bi-layer structure a complete annihilation of the implanted layer makes this relation inapplicable. Under this condition we assumed that the optical absorption of the two layers (implanted and substrate) are identical (thus we consider the limiting condition when the optical absorption coefficients of the two layers become equal). In this case it is important to note that the optical absorption coefficient of phosphorous doped silicon varies as a function of dopaging. According to Labberts and Barkey, however, this variation is very small at short wavelengths (<0.55 μm).[25] For example, at 530.9 nm the difference between an undoped and a high doped sample

Downloaded 08 Dec 2007 to 194.42.23.6. Redistribution subject to AIP license or copyright; see http://jap.aip.org/jap/copyright.jsp

(2×10^{20} cm^{-3}) is less than 15%.[26] In our case, between high and low dose implanted wafers the difference of the carrier concentration is less than two orders of magnitude and thus, we can consider the absorption coefficients, a_i, to be constant. In the case of heavily implanted and highly annealed materials the optical absorption coefficients will not change significantly.

By taking as I_s the PPI signal of the completely recrystallized layer (which is close to the substrate's one, $I_s=5400$, taken from lightly implanted and highly annealed sample: 1×10^{13} P^+/cm^3 and 1100 °C) one can estimate I_i. Looking at the value of I_i on the curves in Fig. 4 corresponding to each dose one can evaluate the defect-annihilation temperature. In fact, each I_i was placed on the abscisa (PPI) and the corresponding temperatures on the ordinate of Fig. 4 were determined for each dose. These data are plotted in Fig. 7. In the same figure, the electrical activation temperatures (obtained by spreading resistance) at which the transition from high resistivity to low resistivity occurs (see Fig. 3) have also been plotted as a function of implantation dose. This last figure confirms our previous conclusions about the electrical activation of such inhomogeneous materials when the total recrystallization is still not achieved. In fact, at low doses of implantation, the decrease of the resistivity is mainly due to a local reconstruction of defects rather than a global amorphous to crystalline transition. We also note that samples implanted at low doses where amorphization did not occur need high defect-annihilation temperatures (see spreading resistance points). On the other hand, heavily implanted samples can be recrystallized at lower temperatures. This is probably due to the fact that spreading resistance is not very sensitive to short range disorder. The defect-annihilation temperatures calculated with the assistance of the above equation show results which are contradictory to spreading resistance measurements. In Fig. 7 the analysis of Raman results through the above equation shows that the defect-annihilation temperature increases with increasing dose. We can therefore conclude that the meaning of defect-annihilation temperature differs according to the technique used. It seems that the Raman signal is more sensitive to local defects in comparison to spreading resistance measurements. In fact, the Raman signal is strongly dependent on the optical absorption coefficient of the implanted layer which depends on point-defect absorption centers. Photons are probably absorbed by electrons which are located in localized band gap states rather than extended state bands. The absorption coefficient is very sensitive even to point defects, while spreading resistance seems less sensitive to those kinds of defects.

VII. CONCLUSIONS

In this paper we have studied the degree of inhomogeneity of implanted materials as well as the kinetics of annihilation of damage as a function of annealing temperature using Raman spectroscopy and spreading resistance measurements. In addition, we have analyzed the reconstruction mechanism of these implanted layers annealed under different isochronal conditions by using a bi-layer model. The main results of our study can be summarized as follows:

(1) The combination of Raman spectroscopic and spreading resistance measurements gives useful information concerning the annihilation of defects in implanted layers.

(2) The phonon peak intensity seems to be very sensitive even for slightly disordered samples such as the ones implanted at low doses (1×10^{13} P^+/cm^2).

(3) After annealing at 700 °C one can observe strong modification of the material. However, total reconstruction can be achieved only at temperatures higher than 800 °C.

(4) There is a strong dependence of the phonon peak intensity on the optical penetration depth of the laser beam.

(5) The Loudon bi-layer model has been successfully used for the estimation of the annihilation temperature for defects in the implanted layers.

(6) A confirmation of a local reconstruction annihilation mechanism rather than an amorphous/crystal transition is also shown.

(7) The Raman signal is more sensitive to local defects than spreading resistance measurements.

[1] J. F. Gibbons, Proc. IEEE **56**, 295 (1968).
[2] J. F. Gibbons, Proc. IEEE **60**, 1062 (1972).
[3] C. Christofides, Semicond. Sci. Technol. **7**, 1283 (1992).
[4] H. Engstrom and J. B. Bates, J. Appl. Phys. **50**, 2921 (1979).
[5] R. A. Forman, M. I. Bell, and D. R. Myers, J. Appl. Phys. **52**, 4337 (1982).
[6] D. Kirillov, R. A. Powell, and D. T. Hodul, J. Appl. Phys. **58**, 2174 (1985).
[7] T. Nakamura and T. Katoda, J. Appl. Phys. **53**, 5870 (1982).
[8] J. H. Hesse and A. Compaan, J. Appl. Phys. **50**, 206 (1979).
[9] Y. I. Nissim, J. Sapriel, and J. L. Oudar, J. Appl. Phys. **42**, 504 (1983).
[10] J. R. Ehrstein, *Nondestructive Evaluation of Semiconductor Materials and Devices*, edited by J. N. Zemel (Plenum, New York, 1979), Chap.1.
[11] C. Christofides, G. Ghibaudo, and H. Jaouen, J. Appl. Phys. **65**, 4840 (1989).
[12] R.G. Masur and G.A. Gruber, Solid State Technol. **24**, 64 (1981).
[13] P.A. Shumann, Jr. and E.E. Gardner, Solid State Electron. **12**, 371 (1961).
[14] U. Fano, Phys. Rev. **124**, 1866 (1961).
[15] F. Cerdeira, T. A. Fjeldly, and M. Cardora, Phys. Rev. B **8**, 4734 (1973).
[16] R. Beserman and T. Bernstein, J. Appl. Phys. **48**, 1548 (1977).
[17] M. Balkanski, J. F. Morhange, and G. Kaneliis, J. Raman Spectroscopy **10**, 240 (1981).
[18] S. A. Kokorowski, G. L. Olson, and L. D. Hess, J. Appl. Phys. **53**, 921 (1982).
[19] B. Boltaks, *Diffusion and Point Defects in Semiconductors* (Mir, Moscow, 1977).
[20] C. Christofides, H. Jaouen, and G. Ghibaudo, J. Appl. Phys. **65**, 4832 (1989).
[21] C. Christofides, G. Ghibaudo, and H. Jaouen, Revue Phys. Appl. **22**, 407 (1987)
[22] J. Said, H. Jaouen, G. Guibaudo, and I. Stoemenos, Phys. Status Solidi A **117**, 99 (1990).
[23] C. Christofides, A. Othonos, J. Boussey-Said, and M. Bisson, J. Appl. Phys. **75**, 3377 (1994).
[24] R. Loudon, J. Phys. (Paris) **26**, 677 (1965).
[25] B. L. Crowder, R. S. Title, M. H. Brodsky, and G. D. Pettit, Appl. Phys. Lett. **16**, 205 (1970).
[26] G. Lubberts and B. C. Burkey, J. Appl. Phys. **55**, 760 (1984).

Downloaded 08 Dec 2007 to 194.42.23.6. Redistribution subject to AIP license or copyright; see http://jap.aip.org/jap/copyright.jsp